JOURNAL OF GEOPHYSICAL RESEARCH, VOL. 102, NO. A12, PAGES 27,083-27,097, DECEMBER 1, 1997

The numerical simulation of VLF chorus and discrete emissions observed on the Geotail satellite using a Vlasov code

D. Nunn, [1] Y. Omura, and H. Matsumoto

Radio Atmospheric Science Center, Kyoto University, Kyoto, Japan

I. Nagano and S. Yagitani

Department of Electrical and Computer Engineering, Kanazawa University, Kanazawa, Japan

Abstract. The Geotail satellite skims the dayside magnetosphere in the equatorial region at about $L = 10$. During such passes the WFC (Waveform Capture Receiver) observes VLF chorus and discrete emissions in the band $200 \sim 1200$ Hz. The most common waveforms observed are rising tones and rising chorus, with hooks and fallers being seen occasionally. Analysis shows that the k vectors are closely parallel to the ambient magnetic field. The Geotail satellite has available comprehensive wave and particle data observed in the vicinity of the generation regions of such VLF emissions. A well-established Vlasov simulation code has been used to simulate the observed emissions, using detailed data from Geotail. The code readily simulates rising frequency VLF emissions with a steep frequency gradient. With appropriate parameter values the code will produce fallers and hooks in good agreement with those observed on Geotail. These self-consistent simulations suggest that nonlinear trapping of cyclotron resonant electrons is the underlying mechanism behind VLF chorus and VLF emissions.

1. Introduction

It has been known for many years that narrowband and band-limited VLF emissions are commonly produced in the Earth's magnetosphere. Such emissions often occur in a ducted or parallel propagating mode, particularly inside the plasmapause, and propagate to the Earth's surface, where they may be readily observed. Early observations of VLF radio emissions [e.g., *Helliwell*, 1965; *Paschal and Helliwell*, 1984; *Carlson et al.*, 1985] were of VLF chorus in the inner magnetosphere, observed on the ground (see, for example, the review of *Sazhin and Hayakawa* [1992]). In recent years satellite observations of both ducted and unducted VLF band emissions have become available [*Burtis and Helliwell*, 1976; *Dunckel and Helliwell*, 1969; *Cornilleau-Wehrlin et al.*, 1978].

VLF emissions may be divided into two categories. The first is the so-called discrete emission (DE), which we here define as an emission having no obvious trigger source and which is apparently an isolated event. DEs may arise spontaneously because of high instability conditions in the plasma or may be triggered by random noise, very weak PLHR, or unducted VLF signals. These occur both inside and outside the plasmapause and may be either ducted and observable on the ground or unducted and observed only onboard a satellite. Discrete emissions are narrowband: sometimes with a bandwidth as little as 10 Hz and consisting of rising or falling tones. Hooks, both upward, and downward are not uncommon. DEs do not seem to have an obvious trigger source, and appear to arise spontaneously because of the nonlinear instability conditions in the plasma. However, a trigger source may be present but unobserved, such as power line harmonic radiation (PLHR) or unducted VLF waves.

The second category of emission in the VLF band is the so-called triggered emission (TE), in which the VLF emission is clearly initiated by a recognizable trigger signal. Triggered emissions are observed to be produced by constant-frequency wave (CW) transmissions from terrestrial VLF transmitters [*Helliwell*, 1965], by lightning VLF whistlers [*Nunn and Smith*, 1996], and by magnetospheric lines and strong PLHR induction lines. In the case of dispersive periodic emissions (PEs) each element is clearly trigged by the two-hop echo of the previous element, and each PE element is thus strictly a TE. In the 1980s, in an inspired experiment, Stanford

[1]Permanently at Department of Electronics and Computer Science, University of Southampton, Southampton, England, United Kingdom.

Paper number 97JA02518.
0148-0227/97/97JA-02518$09.00

University constructed a horizontal VLF transmitter on the south Polar Plateau at Siple station [e.g., *Helliwell*, 1983; *Paschal and Helliwell*, 1984; *Carlson et al.*, 1985]. A variety of CW waveforms were transmitted into the inner magnetosphere, which often triggered VLF emissions in a ducted mode. These were observed at the conjugate point at Roberval Quebec, Canada. During these years a very large and impressive database was built up of the triggered emission phenomenon, in inner magnetospheric ducts. This database may be used to verify nonlinear wave-particle interaction theory and provide evidence of the validity of numerical simulations.

As for discrete emissions and triggered emissions themselves, the salient features seem to be as follows. The k vectors of ducted emissions are closely field aligned, and the k vectors of unducted emissions seem to be field aligned at the point of generation, because the parallel propagation direction is that of greatest instability. Emission bandwidth is typically in the range 10~60 Hz over a large range of L values. Some emissions, particularly fallers, can be astonishingly monochromatic. The emission itself can be a long enduring and stable phenomenon, far outlasting the triggering signal. VLF triggered emissions are also eminently reproducible. The same trigger pulse seconds later will result in an almost identical emission. Emission frequency usually "sweeps," preferentially upwards, at rates that vary from 50 to approximately 2000 Hz/s depending on L shell and other factors. Falling tones are not uncommon, as are upward and downward hooks.

Triggered emissions and DEs generally appear in ground observations and in satellite data as "strong" features, with apparently large amplitudes, often much greater than that of the triggering signal. There has been some difficulty in determining the field amplitudes prevalent in the actual generation region of a VLF emission located in a "duct." It is difficult to extrapolate amplitudes backwards from ground observations to the duct at the equator, and satellite observations have difficulties in that it is unlikely that the satellite will exactly cross the center of a duct. Satellite observations of triggered emissions may either be observing signals leaked from a duct or may be looking at unducted emissions. Observations on the DE 1 spacecraft of Siple VLF transmissions show amplitude observations in the range 0.01 ~ 0.1 pT [*Rastani et al.*, 1985]. Similar observations on IMP6 for June 28, 1973, gave measured wave amplitudes ~0.3 pT [*Inan et al.*, 1977]. In neither case is it entirely clear what the location of the satellite relative to the duct was, or what the linear amplification conditions prevailing at the time were. *Chang and Inan* [1983] in a close study of particles precipitated by a 23 kHz CW signal from a terrestrial transmitter found that equatorial amplitudes ~5 pT gave good agreement with observed particle precipitation. In general, satellites have not been effective at measuring the exit wave amplitudes for VLF emission generating regions located in a magnetospheric duct.

The question must now be asked: What is the plasma theoretical explanation of the origin of radio emissions in the VLF band? Many theoreticians and simulationists have addressed this problem over the last 30 years. Space prohibits a detailed review of much of this work but a good summary is given by *Omura et al.* [1991]. The problem attacked has usually been that of triggered emissions for ducted signals at $L = 4$, owing to the wealth of ground-based observations from the Siple experiment. VLF chorus represents a more complex theoretical problem, in that each "element" has much less coherence than a TE or DE, and the retriggering of the next element is an obviously difficult problem involving recirculation of particles after two bounces and/or retriggering by reflected wave energy from the previous element. However, it would appear that the generation mechanism of a single element of a chorus emission is similar to that of a single TE or DE.

Although the door must not be closed on other mechanisms, it is generally agreed [*Nunn*, 1971, 1974, 1986; *Omura and Matsumoto*, 1982, 1985] that the only feasible process for generating VLF emissions is nonlinear electron cyclotron resonance between energetic electrons with energies ~ keV and narrowband or bandlimited VLF waves. Nonlinearity of the wave-particle interaction process is synonymous with the well-known trapping phenomenon. The theory normally assumes parallel propagation in concordance with ducting theory and with available satellite observations.

Parallel propagating VLF waves with bandwidths < 20 Hz are able to cause nonlinear trapping in the equatorial zone. *Helliwell* [1967] defined a zero net inhomogeneity point or the "phase equator" at $z = s$ where $s = -Adf/dt$. This point is located a distance of the order 1000 km from the equator, and nonlinear trapping must occur within a region of the order 2000 km centered on this point. In addition resonance energy increases away from the equator, causing the population of resonant particles to decrease rapidly.

A fairly simple analysis shows that at Siple latitudes ($L = 4.2$), a minimum averaged wave B field amplitude in the equatorial generation region of about 2 pT is required to effect trapping and nonlinear wave-particle interaction. Theoretical analyses by *Nunn* [1974] showed that, if this criterion is satisfied, the nonlinear wave-particle interaction process in a parabolic inhomogeneity could indeed produce emissions in the VLF band. The full nonlinear self-consistent problem is obviously very complex and requires numerical simulation for further elucidation. One-dimensional (1-D) Vlasov simulations by *Nunn* [1990, 1993] and *Nunn and Smith* [1996] reproduced triggered VLF emissions in agreement with observation. We must underline the fact that it is at the equator that field amplitudes need to be > 2 pT, and the exit amplitudes will also be of this order. The input triggering signal introduced at the upstream end of the simulation box can be very small. This signal will be linearly amplified to nonlinear amplitudes during the time it propagates to the equator. In the Siple simulations of *Nunn* [1993] the integrated linear amplification across the simulation box was ~ 32 dB, which is in good agreement with figures quoted by *Helliwell* [1983]. When a self-consistent nonlinear generation region is es-

tablished, the plasma is in a state of nonlinear absolute instability. Then no field input at all is required and the wave amplitude at the equator is determined by the GR structure.

A rather different approach was adopted by *Carlson et al.* [1990], based upon observations detailed by *Paschal and Helliwell* [1984] and *Carlson et al.* [1985]. *Carlson et al.* [1990] assumed a parabolic inhomogeneity in $B_o(z)$ and obtained good agreement with initial observed phase behavior, as well as saturation at the trapping level at amplitudes of about 2 pT. Such behavior is characteristic of the homogeneous problem. Their simulation code, while interesting, assumes a particle distribution which is coarsely distributed in parallel velocity, and it is difficult to see the relevance of this situation to the VLF emission problem. Here we must be dealing with a continuous distribution function which is anisotropic over a sizable region of velocity space, since triggered emissions sustain themselves over a frequency range ~kHz.

It should be realized that there are outstanding problems associated with these 1-D simulations. The saturation mechanism and nonlinear loss processes are ill understood, and require a 3-D simulation and possibly the intervention of electrostatic wave instability as well. The slow exponential growth phase in the triggering of an emission by a weak key down signal remains mysterious, but plausible theories have been advocated by the Stanford group. But above all, the simulations assume B wave field amplitudes in the generation region $\geq$ 2 pT and suppose an energetic electron distribution function of a bi-Maxwellian or loss cone type that is linearly unstable with a growth rate $\geq$ 70 dB/s (for Siple TE simulations). Such assumptions have never been satisfactorily validated by satellite observations at the generation region site.

With the launch of the Geotail satellite 3 years ago an opportunity presented itself to test 1-D Vlasov simulation codes and nonlinear wave-particle interaction theory against detailed wave and particle observations. In skimming the dayside magnetosphere at $L = 10$ in the equatorial zone, Geotail observes VLF rising chorus, rising frequency DEs, and occasionally falling frequency DEs and hooks. As well as detailed wave observations, Geotail provides remarkably good data on electron distribution functions, and all this in the close vicinity to the generation region of these VLF emissions. Analyses at Kanazawa University show that while the k vectors of these emissions are usually close to parallel with the ambient B_o field, the waves appear to be unducted, since the k vectors veer steadily away from the B_o direction as they propagate away from the equator. At $L = 10$ then, we should not have the problem of the emission generation region being confined to a small duct that the satellite is unlikely to penetrate.

In this paper we shall take a well-established 1-D Vlasov Hybrid Simulation (VHS) code [*Nunn*, 1990]. The code will be modified to suit the environment at $L = 10$, and a number of updates will be made. Using all the parameters measured by Geotail, a number of specific VLF emission events observed on Geotail will be simulated as closely as possible. With the proviso that there is considerable uncertainty over the exact instantaneous electron distribution function, the code will be found to successfully reproduce the kinds of VLF event observed on Geotail. The fit of Geotail observations to the established theory will be found to be very good. The aim of this paper, then, may be regarded as first to investigate and understand better the physics of nonlinear wave-particle interaction in the outer magnetosphere and, perhaps more importantly, to verify the underlying hypothesis that nonlinear electron cyclotron resonant trapping is indeed the root cause of emissions in the VLF band.

2. The Geotail Satellite

The Geotail orbit is such that it skims the dayside magnetosphere in the equatorial region at $L = 10$. During the majority of such passes VLF chorus or discrete emissions are observed [*Nagano et al.*, 1996]. The Geotail spacecraft simultaneously measures the EM wave field and electron distribution function. In this paper we shall only present frequency/time spectrograms for a few chosen VLF emission events. To obtain details of the spacecraft instrumentation, and for comprehensive analysis of the data, the reader is referred to the publications of the principal investigators [e.g., *Frank et al.*, 1994; *Kokubun et al.*, 1994; *Matsumoto et al.*, 1994a; *Mukai et al.*, 1994; *Williams et al.*, 1994; *Frank et al.*, 1996].

2.1. The VLF Wave Measurements

The plasma wave instrument (PWI) on board Geotail is a powerful tool to analyze the wave propagation of chorus emissions, since it has the waveform capture facility (WFC) which acquires two electric and three magnetic components of the EM field. For technical details of the instrumentation see papers by *Kokubun et al.* [1994], *Matsumoto et al.* [1994a] and *Tsutsui et al.* [1996]. From the WFC, exact wave normal and Poynting directions may be obtained, as well as the detailed frequency/time structure in the band from 10 to approximately 4000 Hz. This amply covers the frequency range of observed emissions. Wave vector and Poynting vector analysis by *Nagano et al.* [1996] reveals a spread of k vectors largely confined to directions within 20° of the ambient field direction. It has also been observed [*Yagitani et al.*, 1996] that these VLF waves appear to be unducted, in that the k vectors drift away from the B_o direction as they propagate away from the equator. In our simulations we shall assume that the k vectors are strictly parallel in the generation region and that the small propagation angles observed on Geotail arise from unducted propagation from the generation region to the spacecraft.

2.2. The Particle Observations

At the exact time of a chosen chorus event the simulations in this paper require measurement of low-energy electron density (or "cold" plasma density) and electron

cyclotron frequency. Also required is the distribution function of the hot electron component in the energy range 6 – 60 keV, which covers the range of resonant energies for Geotail chorus events. The comprehensive plasma instrument (CPI) on Geotail [*Frank et al.*, 1994] provides such plasma data simultaneously with the field measurements.

Recent analyses of Geotail particle data are given by *Yagitani et al.* [1996] and *Frank et al.* [1996]. To obtain meaningful data from the particle counters, Geotail distribution function measurements are 24-s averages. Inspection of the data by *Yagitani et al.* [1996] shows that a typical observed time averaged distribution function favorable for chorus generation may be modelled by the following function of energy W and equatorial pitch angle α

$$F(W,\alpha) = AW^{-n}\{a + \sin^m\alpha\} \quad (1)$$

where $n \sim 3.3$, $m \sim 3$, and $a \sim 0.33$. We shall use distribution function models of this form in the simulations. When the observed distribution function is integrated over α and presented as a function $G(W)$, very frequently there is an inflexion in the $G(W)$ curve in the region of 20 keV, and a range of energies in which the gradient $\mathrm{d}F/\mathrm{d}W$ is considerably reduced [*Yagitani et al.*, 1996]. Such an inflexion would give greatly enhanced linear growth rates over a finite frequency band.

3. VLF Emission Events Observed on Geotail

VLF emission events observed on Geotail may be divided into the following categories:

1. Quasi-broadband unstructured emissions. These will not be considered in this paper since the corresponding wave particle interaction processes will be linear [*Nunn*, 1984].
2. Rising frequency chorus, with broad swishy individual elements. This category of emission seems to be the most common [*Nagano et al.*, 1996]
3. Rising frequency discrete emissions. These are fairly common, and are strong features with narrow bandwidth and steep frequency gradient. They often occur in groups.
4. Falling frequency discrete emissions. These are less common and have lower amplitudes and sweep rates than the risers.
5. Discrete emissions with upward and downward hooks. These are not common but are sometimes observed.

Since the simulation code is limited to a bandwidth ~ 40 Hz, we now select two typical DE events for detailed analysis and simulation.

4. Spectrograms of Selected VLF Emission Events

4.1. Event R

Plate 1 shows the spectrogram for this event. Appropriate data are set out in Table 1. This spectrogram shows a number of steep risers, with maximum amplitudes in the region of 150 pT and B_{rms} field values ~ 50 pT. Sweep rates are all about 600 Hz/s. Of particular interest are the upward hook like features at $t = 4$ s.

4.2 Event F

Plate 2 shows the spectrogram of a weak, slow falling tone. Data for this event is given in Table 1. This event is interesting but unusual, and was first shown by *Nagano et al.* [1996], who have other examples of fallers. Fallers are relatively infrequent however. The amplitude of the B field envelope is available for this falling tone. The maximum value is about 20 pT and is remarkably constant. As lower frequencies are reached the growth rate falls off and the emission amplitude steadily declines, and eventually the emission ends at about 200 Hz. The bandwidth of the emission is about 20 Hz, and sweep rate is low, at −50 Hz/s. By Geotail standards this is a very long lasting emission, with a duration of about 4 s.

5. The Simulation Code

The code simulates numerically the self-consistent nonlinear cyclotron resonant interaction between a band-limited VLF wave field and a "hot" anisotropic distribution of electrons. The spatial domain of the simulation is in the equatorial region where nonlinear trapping is possible and where the resonant energy is lowest. The code is 1-D and assumes propagation parallel to the ambient field (coordinate z). It should be noted that it reproduces exactly linear behavior in the low-amplitude regime: indeed, in this case code output will be fairly precise since nearly all the approximations in the code appertain to the nonlinear case.

The code employs a simulation technique called Vlasov Hybrid Simulation (VHS), which is well suited to the problem at hand. In this paper only a general discussion of the code will be given. Mathematical details are given by *Nunn* [1990]. *Nunn* [1993] describes the VHS method in very general terms, and *Nunn and Smith* [1996] describe recent updates and give simulations of whistler-triggered emissions.

5.1. The Field Equation

Since the simulation is band limited, the code defines a base frequency ω_o and base wave number $k_o(z)$. This fast phase variation is divided out, allowing us to define a complex dimensionless amplitude $\tilde{R}(z,t)$ and the corresponding dimensionless resonant particle current $\tilde{J}(z,t)$. The dimensionless analysis uses $1/\bar{k}$ as the unit of length, where $\bar{k} = \Pi_e/c$, and $1/\bar{\omega}$ as the unit of time, where $\bar{\omega} = \Omega_e/2$, Ω_e is electron gyrofrequency, c is the velocity of light, and Π_e is the electron plasma frequency. All subsequent equations are in dimensionless units. Under the assumption that $\tilde{R}(z,t)$ is slowly varying (narrow band approximation), Maxwell's equations and the linear equations of motion of the cold plasma furnish the field equation

$$\left(\frac{\partial}{\partial t} + V_g\frac{\partial}{\partial z}\right)\tilde{R} = -\frac{\omega_o V_g}{k_o}\tilde{J} - \gamma_{NL}(|\tilde{R}|)\tilde{R} \quad (2)$$

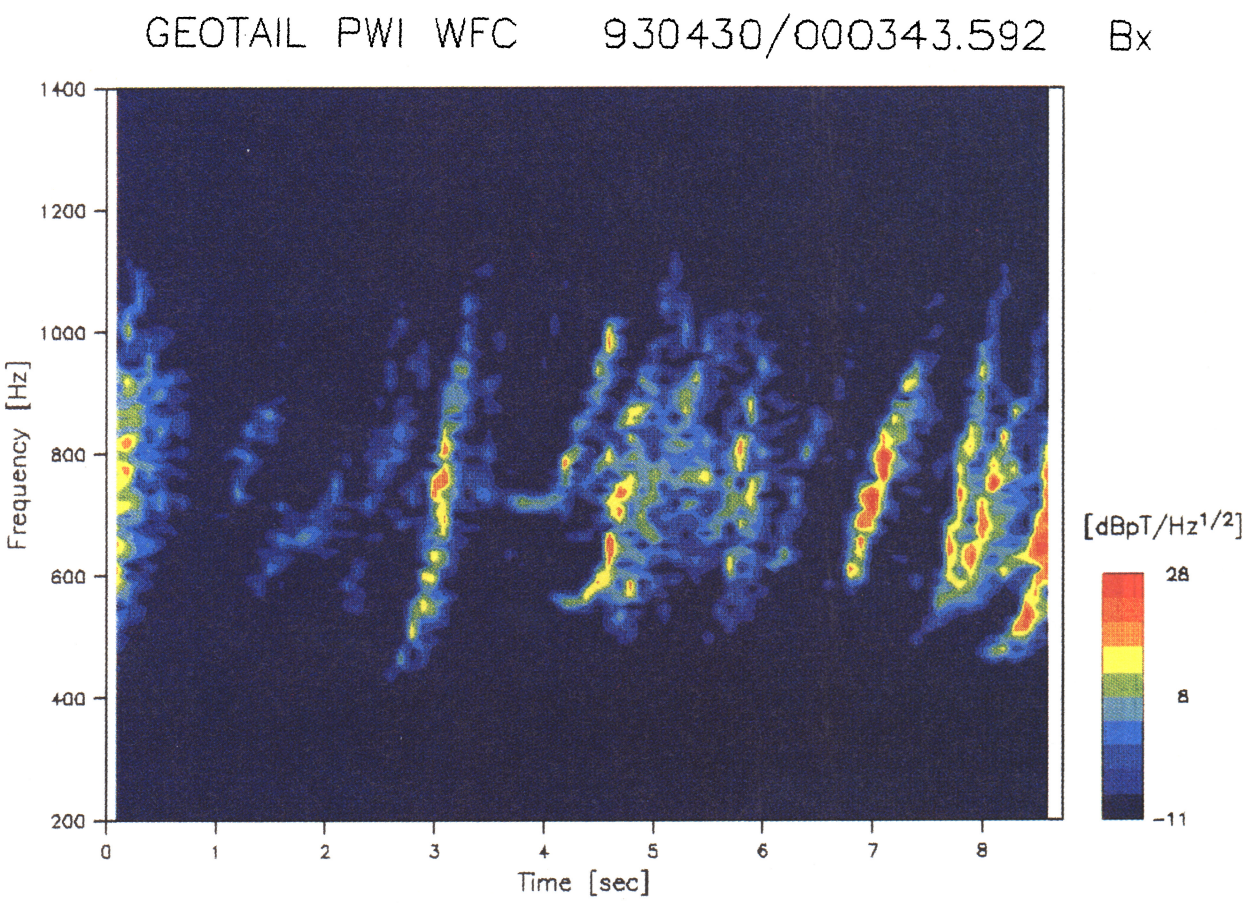

Plate 1. Event R. Strong rising chorus and some upward hook events.

where V_g is the group velocity and the last term models nonlinear unducting loss.

Note that for VLF emission/chorus simulations, the average frequency changes over a wide range. During the simulation the base frequency is continually redefined. The ambient magnetic field is assumed to have a parabolic dependence on z:

$$B_o(z) = 1 + 0.5\chi z^2 \tag{3}$$

where $z = 0$ is at the B_o minimum, and scale factor χ, in the absence of more precise information, is chosen to be that appropriate to a dipole field at $L = 10$. The minima of both B_o and electron density N_e are taken to be the values actually measured on Geotail.

Table 1. Data for VLF Emissions

Item	Event R	Event F
Date	930430	921017
Time, UT	00:03	22:05
Spacecraft position		
Y_{sm}, R_E	−4	−9
X_{sm}, R_E	+6	+6
Electron gyrofrequency, Hz	2850	1200
Electron plasma frequency, Hz	13000	7500
Cold plasma density, per cm^3	2.1	0.7

Observations by *Morrison et al.* [1994] and *Tsurutani et al.* [1977] show that considerable field line distortion may occur at $L = 10$ on the dayside, giving two or even three distinct B field minima. It is noticed that Geotail VLF chorus is usually associated with the single B_o minimum nearest to the satellite. The two data examples in this paper were both on the morning side, where multiple minima are less likely. Accordingly, the simulations in this paper are to be regarded as applying to the single B_o minimum nearest to Geotail for the event in question, and since the signals are unducted they are unlikely to reach any other minimum. From Geotail measurements the exact shape and location of the nearest minimum is unknown, but the simulation results are not sensitive to these quantities.

5.2. The Saturation Mechanism

In simulating VLF emissions we are dealing with a plasma that is absolutely unstable in the nonlinear regime. For a 1-D code with a parabolic inhomogeneity there is nothing to limit the growth of the wave field. This is different from the homogeneous problem where nonlinear trapping limits growth. For a 1-D code it is necessary to insert amplitude saturation phenomenologically. The most likely physical mechanism is as follows. The nonlinear current $\tilde{J}$ is actually 3-D and on wave number decomposition will be found to radiate into a broad spectrum of wave numbers. Energy ra-

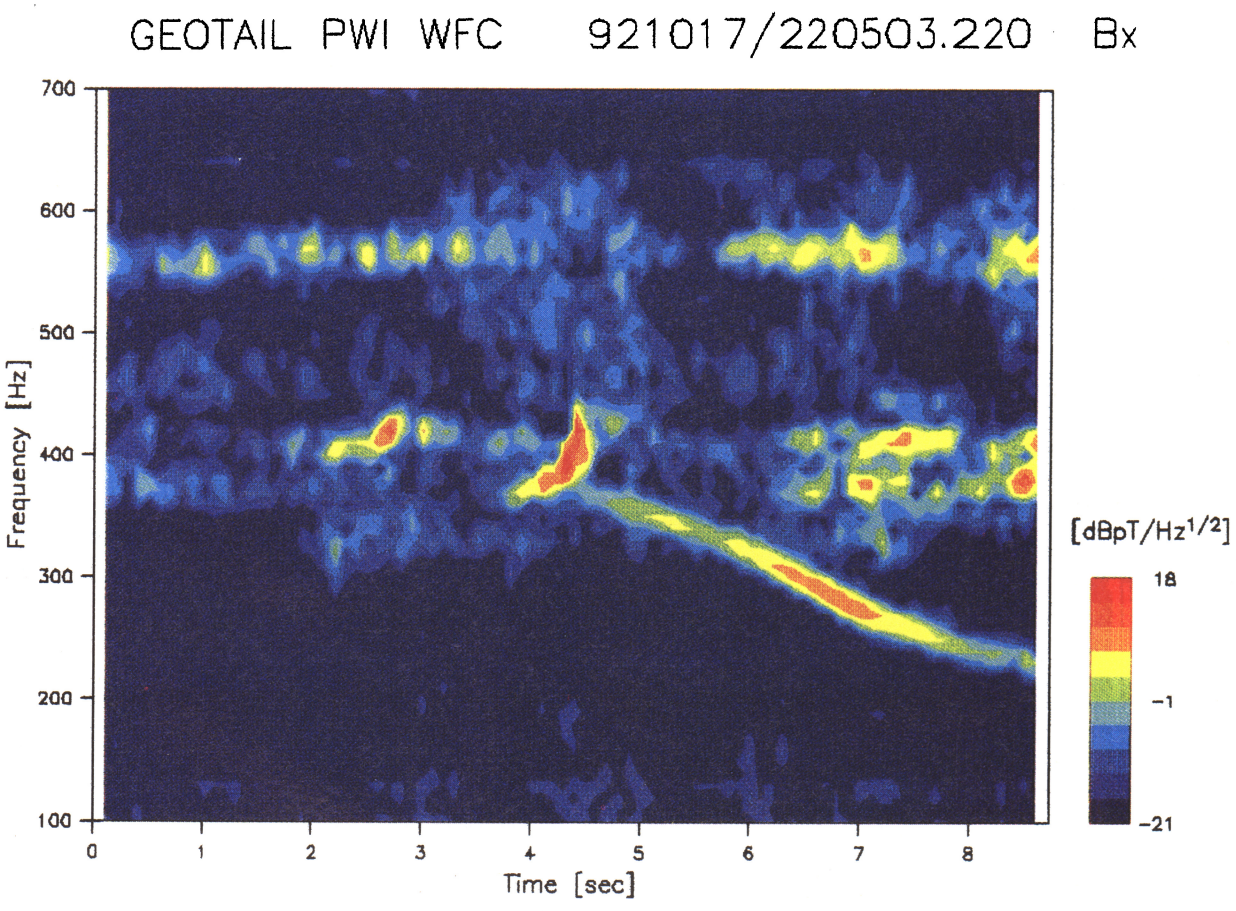

Plate 2. Event F. A weak falling tone with a low sweep rate. This is a very long enduring emission, lasting 5 s.

diated into nonparallel directions will propagate laterally away from the generation region and be Landau damped, thus providing a mechanism for power loss. Another physical mechanism may also be operative. Nonlinear trapping in inhomogeneous media generates a hole (or a hill) in the distribution function. Electrostatic waves with phase velocities on the upper side of phase averaged distribution function, or vice versa, will experience large linear Landau growth rates. The resulting electrostatic wave field will quench gradients in the V_z direction and thus reduce cyclotron growth rates. Neither mechanism is understood in detail at present and both require simulations with complex 3-D codes currently beyond the reach of computer technology.

The saturation term $\gamma_{NL}\tilde{R}$ is shown in (2) as an extra damping. The nonlinear damping rate increases rapidly above some level $|\tilde{R}| = R_{\max}$, normally chosen to fit observed amplitudes. Even if γ_{NL} is a function of a weighted average of $|\tilde{R}|$ over the whole z domain, this saturation mechanism will bias the spectrum, tending to broaden and flatten it. Here we have developed a new nonlinear loss term, applied in the Fourier domain. If $\{R_k\} = \text{FFT}\ \{\tilde{R}(z_i)\}$ is the spatial FFT of the $\tilde{R}$ field on the z grid, we may update the spatial spectrum R_k at each time step by

$$R'_k = R_k - \gamma_{LIN}\Delta t G(\bar{R}) H(R_k) R_k \qquad (4)$$

where γ_{LIN} is the linear growth rate at the equator $z = 0$, G is a function of global average wave amplitude $\bar{R}$ that rises steeply for $\bar{R} > R_{\max}$, and $H(R_k)$ is a function that biases the spectrum. This is a fairly general loss mechanism, but it was found that the results using this were little different from those obtained using (2). It appears that the exact details of the saturation mechanism are unimportant. For weaker linear growth rates it is possible to run the code and trigger emissions, without invoking the saturation mechanism. All "strong" triggering effects do require however a sink for wave energy if the process is going to be visualized as being 1-D.

5.3. The Ambient Plasma

The low-energy electron plasma(< 1 keV), whose density is directly measured by Geotail, is linear and for modeling purposes may be represented as being a cold plasma, density $N_e(z)$. The dependence of $N_e(z)$ upon z is not critical, but is here assumed to be parabolic

$$N_e(z) = N_e(0)(1 + 0.5\nu z^2) \qquad (5)$$

where ν is a constant of proportionality which determines the functional dependence of $N_e(z)$ on $B_o(z)$. Ions are assumed to be immobile. The unperturbed hot electron distribution function is specified in dimen-

sionless units by $F_o(\mu, W)$, where W is energy and μ is magnetic moment. Note that all distribution functions in this paper are defined with respect to linear r, v phase space. The above F_o is not particle density in $\mu - W$ space! The free energy for the instability must derive from the anisotropy of F_o. To simulate emissions/chorus we require a linearly unstable plasma and a positive linear growth rate since nonlinear and linear growth rates are normally of the same sign: nonlinear growth rates being typically larger by a factor of 2~5.

The main task of the code is to compute the nonlinear resonant particle current $\tilde{J}(z,t)$, which is the source current or "antenna" in the field equation and generates the emission. Making the valid assumption that ΔW is small, the formal expression for $\tilde{J}$ is, in dimensionless units,

$$\tilde{J}(z,t) = \frac{2\bar{k}^3}{N_e} \int_{V_\perp} \int_{\psi} \int_{v^*} e^{i\psi} \Delta W F_o' V_\perp^2 dv^* d\psi dV_\perp \quad (6)$$

where

$$F_o' = \left\{ \frac{\partial F_o(\mu, W)}{\partial W} + \frac{2}{\omega_o} \frac{\partial F_o(\mu, W)}{\partial \mu} \right\}_{V_z = V_{\rm res}} \quad (7)$$

The quantity ΔW is the integrated energy change of a test particle at that point in phase space. The variable ψ is gyrophase, and $v^* = V_z - V_{\rm res}$ is parallel velocity about resonance. The v^* integral must be evaluated for a narrow range centered on the cyclotron resonance velocity $V_{\rm res}(z,t)$ at the center frequency of the local wave field . It is seen that the driver for the instability is the gradient term F_o', which may be viewed as a function of z, $|V_\perp|$, and local mean frequency $\bar{f}(z,t)$. A specific chorus event is driven by positive gradients F_o' in a restricted region of velocity space, corresponding to the appropriate range of resonant velocities.

5.4. The Frequency Sweep Rate Mechanism

The code will be found to simulate the sweeping frequency of VLF emissions. It is a matter of considerable intellectual curiosity as to how this sweeping frequency comes about. A phenomenological approach to the frequency shift problem was advanced in *Helliwell* [1967]. Helliwell associated the zero inhomogeneity point (or the so-called phase equator) with the generation region location, which thus became a function of sweep rate. This hypothesis is only approximately true, since the zero inhomogeneity point will be a function of perpendicular velocity, and the generation region (GR) itself will have a finite size. In fact the condition for optimum nonlinear wave growth is that $0.3 < |S/R| < 0.8$, where S is the net inhomogeneity factor [*Nunn*, 1974] and R is wave amplitude. This is at variance with Helliwell's assumption that the condition $S = 0$ gives greatest growth. In addition the Helliwell theory gives no details of the plasma physical mechanism whereby wave phase is actually changed.

In the framework of nonlinear theory we proceed as follows. If we define $\tilde{R} \equiv Re^{j\phi}$, then ϕ is the additional phase over the base phase. Some manipulation [*Nunn*, 1990] of (2) gives the result

$$\frac{\partial \omega}{\partial t} = \frac{\partial^2 \phi}{\partial t^2} = V_g^2 \frac{\partial^2 \phi}{\partial z^2} + \frac{V_g^2 \omega_o}{k_o} \frac{\partial}{\partial z} \left(\frac{J_i}{R} \right) - \frac{\omega_o V_g}{k_o} \frac{\partial}{\partial t} \left(\frac{J_i}{R} \right) \quad (8)$$

where J_i is the component of $\tilde{J}$ parallel to the local wave $B_\perp$ field. It is important not to jump to any hasty conclusions from this equation. First, the frequency shift mechanism must be nonlinear, and a self-consistent solution of the wave equation is necessary to unambiguously establish the frequency shift. However, a cursory glance at this equation tells us where the shift comes from. The last term cannot give shifts of more than a few Hz. The driver term is the second one. It has been shown that nonlinear trapping in parabolic inhomogeneities can result in significant value for the global average of $\Phi = \partial/\partial z(J_i/R)$ [*Nunn*, 1974]. For a VLF emission generation region confined mainly to the region downstream of the equator, with typical Siple parameters, a positive value $\partial w/\partial t$ of $\sim +200$ Hz/s, from the second term, would be the best that could be achieved. For a generation region profile extending well upstream of the equator a value of -200 Hz/s is typical. Past experience with the code at $L = 4$ suggests that observed sweep rates of the order of $\pm$ 1 kHz/s or more can only be achieved if the first term, which is purely advective, is significant. To achieve sweep rates with an advective term may appear underhand. However a strongly nonlinear $\tilde{J}$ is required to (1) establish a generation region with a wave number gradient across it and (2) maintain it in a constant position on the field line [*Nunn*, 1984]. However, the set up process is dynamic, very complex, and only accessible by simulation. It is clear that the quantity $\partial\Phi/\partial z$ is mainly instrumental in setting up such wave number gradients.

5.5. Filtering of the Simulation Field

At each time step the field values on the z grid, $\tilde{R}(z_n)$, must be spatially bandpass filtered to the simulation bandwidth of $\sim$ 40 Hz, which amply covers experimentally observed bandwidths. To allow the center frequency of the band to be a function of z, we employ the following filtering procedure. At each time step t_n the local center wave number $\tilde{k}(t_n, z)$ is estimated. A function $k_m(z)$ which is a polynomial in z of order m, is defined, and a least mean squares fit to $\tilde{k}$ is found. A matched filter is employed as follows [*Nunn and Smith*, 1996]. The phase variation due to $k_m(z)$ is divided out from $\tilde{R}(z)$, and then $\tilde{R}$ is bandpass filtered to $\pm$40 Hz using a spatial FFT and IFFT of $\tilde{R}(z_n)$. The phase variation due to $k_m(z)$ is then added back into $\tilde{R}$. Of course spatial gradients in frequency/wave number could be accommodated by a much larger overall simulation bandwidth of $\sim$ 150 Hz. However, since the code run time goes as bandwidth cubed, this option is out of the question.

5.6. The Vlasov Hybrid Simulation Method

A 4-D phase box is defined in the variables z, $|V_\perp|$, ψ, and $v^* = V_z - V_{\rm res}$. The box range in z is fixed from $z_l \rightarrow z_r$, where z_r is positive and is the wave exit side. The box size in z is chosen to be the smaller of the following: (1) the zone of nonlinear trapping, assuming $|\tilde{R}| = R_{max}$, or (2) the region where linear growth rate is > 0.05 times the equatorial value. In the present simulations (2) is always smaller.

This code uses two grids, one for particles with N_j points, the other for fields with N_k points. The simulation time step $\Delta t = \Delta z_j/|V_{\rm res}| = \Delta z_k/V_g$ where $\Delta z_j = (z_r - z_l)/N_j$ is the spacing of the particle grid, and Δz_k is the field grid spacing. Clearly, $N_k/N_j = |V_{\rm res}|/V_g$. The number of grid points N_j needs to be chosen such that (1) the particle equations of motion are integrated to a sufficient degree of accuracy, which requires that $\Delta t/T_{tr} < 1/20$, where T_{tr} is the minimum trapping time in the system, and (2) the number of field grid points N_k needs to be large enough to resolve the global simulation bandwidth without aliasing. For the cases of runs A and C, $N_j = 1600$ satisfied the above criteria with $\Delta t/T_{tr} = 1/25$. Run B is a much weaker event with a much longer trapping time, and a value of $N_j = 512$ satisfied the above criteria with $Deltat/T_{tr} = 1/30$. Experimentation with short production runs showed that these grids gave a stable result.

The range in parallel velocity $v^*, v_1^* \rightarrow v_2^*$, spanned by the phase box is a function of z and t, and is centered on the local resonance velocity $V_{\rm res}(z,t)$. The width $v_2^* - v_1^*$ covers the range of resonance velocities for the simulation bandwidth plus two nonlinear trapping widths. The number of grid points in v^* is N_{v^*}.

The variable ψ is gyrophase with N_ψ grid points. It necessary to resolve adequately the distribution function in $v^* - \psi$ space, where the dominant structure is usually the resonant particle trap. Extensive numerical experiments have shown that $N_{v^*} = 40$, $N_\psi = 20$ provides adequate resolution and a stable result and these values were used throughout.

Through the variable v^* the phase box is a function of time and is matched to the local field in space and time.

The coordinate $|V_\perp|$ is relatively insensitive in this problem. The contribution to current $\tilde{J}$ from each discrete value of $|V_\perp|$ is calculated entirely separately in this program. The range of $|V_\perp|$ values required in the simulation is quite narrow, corresponding to a pitch angle range from 40 to 65°. Low pitch angle particles are linear, and the numbers of particles at very high pitch angles is small. The production runs in this paper will be done with 10 values of $|V_\perp|$, but experimental runs may be done with 3 values of $|V_\perp|$, or indeed 1. Enough grid points are needed to resolve the functional dependence of F_o' on $|V_\perp|$. It is also necessary to have enough grid points to span the whole range of $|V_\perp|$ where F_o' is significant, in order for there to be a range of trapping frequencies present. This is needed to reproduce the sideband stability characteristics correctly.

The main task of the code is to calculate current $\tilde{J}$ in (6) using the VHS algorithm. The main features of the algorithm are as follows:

1. At time $t = 0$ the phase box is filled with particles with a density of about 1.2 per grid hypercube.

2. The code follows each particle's trajectory in the phase box. Each particle is embedded in the Vlasov fluid. The whole method is based upon the integral form of the Vlasov equation, or Liouville's theorem. The well-known Vlasov codes of *Cheng and Knorr* [1976] and *Denavit* [1972] integrate the Vlasov equation directly, a procedure which requires smoothing of the distribution function since derivatives in velocity space are involved. Liouville's theorem tells us that F is conserved along these phase trajectories, but the code actually computes ΔW (effectively δF) along each trajectory. What the code is essentially doing is computing a large number of continuous phase space trajectories within the phase space box.

3. At each time step ΔW is interpolated from the particles to the phase space grid, using the following algorithm

$$\Delta W_{ijk} = \left(\sum_\ell \Delta W^\ell \alpha_\ell\right) / \left(\sum_\ell \alpha_\ell\right) \qquad (9)$$

where the sum ℓ is over all particles in cells adjacent to grid point ijk, ΔW_ℓ is ΔW for the lth particle, ΔW_{ijk} is the value at grid point ijk, and the α_ℓ are area or volume weighting coefficients. The density of the simulation particles themselves is conserved along a phase trajectory, and there is no tendency for them to bunch in phase space. This density must be held above a certain minimum value in order for the interpolation procedure to work. Any density above this floor is permissible, and particles may be inserted into the phase fluid or removed at will. This is a feature not shared by any other simulation method.

4. With ΔW_{ijk} now defined on the grid, the integral for $\tilde{J}$ in (6) is readily evaluated.

5. Particles leaving the phase box (relative to coordinate v^*) are nonresonant with the local wave field and are discarded from the simulation. New particles have to be inserted into the phase fluid on the edge of the box where phase fluid is flowing in. This operation requires some care.

6. The unperturbed distribution function F_o is introduced at $z = z_r$, and the wave field exiting the box at $z = z_r$ is collected up into an array for graphical processing.

The VHS method is very suitable for the VLF emission problem where the resonance velocity changes drastically with position and time. Vlasov methods generally are low noise, particularly when $\delta F \ll F$, since it is effectively δF that is pushed. Particle-in-cell methods can be used for VLF wave-particle interaction simulations, but they are best for situations where the frequency does not change by a great amount. They have the advantage that nonresonant particles are not dis-

carded, and thus PIC codes can look at particle diffusion, and given enough computer time can recirculate particles after two bounces [*Omura and Matsumoto*, 1982, 1985].

5.7. The Numerical Simulations

Before presenting the actual results a number of general points need to be made. The first concerns the unperturbed distribution function of energetic electrons, $F_o(\mu, W)$, which we take to be a function of energy W and equatorial pitch angle α. Referring to the 24-s average distribution functions seen on Geotail, observed distributions favorable for chorus generation can be well modeled by (1). If the constant A is chosen to agree with observed particle densities in each energy band, we end up with a linear growth rate at the equator of order 10 dB/s. If the code is run with such a distribution function triggering will not take place. Extensive experimentation revealed that for a wide range of other parameters, a minimum linear equatorial growth rate(at the starting frequency) of 40 dB/s is required for triggering. The reason for this is that a VLF emission is produced by a nonlinear structure or GR in a stationary position on the field line. The minimum growth rate is necessary to keep the GR amplitude profile in a constant position. With growth rates above 40 dB/s the code almost always triggers and effectively exhibits a nonlinear absolute instability to band limited VLF waves.

It was pointed out by *Yagitani et al.* [1996] that a distribution function (with $\gamma_{LIN} > 40$ dB/s) is unlikely to remain in a state of absolute instability for periods of 24 s plus. It thus seems likely that VLF chorus/emissions are caused by transient increases in linear growth rate, which may be due to injected particles or bouncing particle bunches. Close inspection of the particle data reveals that the energy dependence of F_o often has a "ledge" in the region of 20 keV where the fall off with energy is much slower. This is in the vicinity of the resonant energies for VLF chorus at $L = 10$. Now an energy dependence of the form W^{-3} is very damaging to the wave-particle interaction process, reducing the anisotropy to very low levels. With a falloff as W^{-2}, however, anisotropy is greatly increased and linear growth rates $\sim$ 60 dB/s may be obtained with particle densities close to observed values.

We will assume that the VLF chorus/emissions are caused by distribution functions that are localized in time, and the instability is due to a localized region in velocity space, matched to the resonant velocity range for the emission, where the gradients of F_o are more favorable for linear and nonlinear growth. The code will be driven by a distribution function of the form in (1), with typical values of $a = 0.33$, $m = 3$, and $n = 1.4$. The constant A is chosen to match observed energetic particle densities, which will give linear growth rates of 60$\sim$ 80 dB/s. Essentially we are modeling F_o in a limited region of velocity space near the "ledge." It is perhaps rather unfortunate that it is not practical to measure distribution functions on a time scale of the order of 1 s.

The second point to emphasize is that wave amplitudes observed on Geotail correspond to very strong nonlinearity and trapping of electrons for many trap-

Table 2. Data Used for Simulation Runs

Item	Run A	Run B	Run C
L shell	10	10	10
Electron gyrofrequency, kHz	2.8	1.2	2.8
Plasma frequency, kHz	13	7.777	13.014
Cold electron density, per cm^3	2.10	0.75	2.10
Refractive index	11.44	13.9	11.45
Start (base) frequency, Hz	588	384	588
Parallel resonance energy, keV	27.7	5.9	27.6
Total resonance energy, keV	40 $\sim$ 200	12 $\sim$ 30	48 $\sim$ 100
Linear growth rate at $f = f_o, z = 0$, dB/s	85	50	120
Electron density 30 $\sim$ 48 keV, per cm^3	0.0024	0.0024	0.0034
Global anisotropy	0.89	0.807	0.8107
Loss process domain	frequency	time	time
Saturation level B_{max}, pT	160	25	160
Bandwidth/matched filter, Hz	63	12	47
Bandwidth global filter, Hz	400	104	309
Number of points in $V_\perp$	3	10	10
Number of points in v^*	40	40	40
Number of points in ψ	20	20	20
Pitch angle range	33 $\sim$ 72°	45 $\sim$ 77°	45 $\sim$ 60°
Points in z grid (particles) N_j	1600	512	1600
Points in z grid (field) N_k	3825	801	3825
Total particles (approximately)	3,840,000	4,000,000	4,000,000
Trigger signal: broadband noise, pT rms	0.7	0.7	0.7
Spatial variation of $\bar{f}(z)$	linear	linear	linear

ping periods. This is even true for the relatively weak faller event shown.

The third point is that steep risers are the most common form of emission observed. This is exactly what the code produces when fed with "typical" Geotail parameters.

5.8. Simulation of Steep Rising Frequency DE: Event R

The first simulation (run A) will be of a strong steep riser, and is an attempt to simulate event R. Data used in the simulation is shown in Table 2 and should be self-explanatory. The input trigger signal introduced at the upstream end of the simulation box at $z = z_l$ is weak broadband noise occupying the simulation bandwidth. With the parameters L, N_e, Ω_e and $B_{\max}$ set for this event, the code consistently triggered stable risers. Figure 1 shows the f/t spectrogram of the wave field exiting from the simulation box at $z = z_r$. This is in the form of a shaded contour plot of spectral power. The FFTs are Hamming weighted with a frequency resolution of 4 Hz. Two strong risers are triggered, with the frequency sweeping from $f = 600$ Hz to $f = 1100$ Hz in about 0.7 s. In this example the simulation is reset after the first riser, and the second riser is produced starting from weak broadband noise within the simulation bandwidth. The sweep rate of about +800 Hz/s is in very good agreement with observations. This kind of behavior is readily reproducible and occurs with a wide range of code parameters, and also with a totally different nonlinear loss mechanism. The plasma is effectively absolutely unstable in the nonlinear regime, in that any kind of noise or signal in the simulation band will rapidly grow and trigger a stable long enduring emission. The resulting emission is more or less independent of the details of the trigger signal. For this simulation the integrated linear growth rate across the simulation box is 63 dB. The weak input signal is linearly amplified while propagating to the equator by some 31.5 dB, at which point nonlinear amplitudes are reached and the GR is set up. Once the GR is established the system is in the absolute instability mode and no input signal is required. It must be reemphasized that the input signal is weak. The nonlinear trapping amplitudes exist only in the equatorial region, the exit wave amplitudes are of this order.

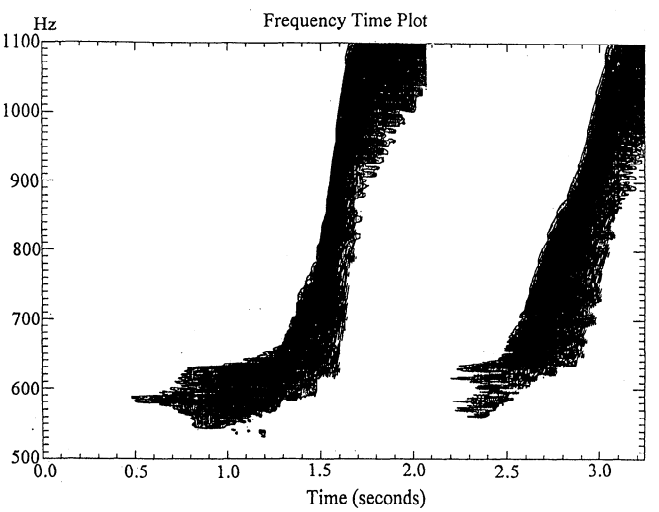

Figure 1. The f/t spectrogram of simulated rising frequency discrete emission (run A) presented as a shaded contour plot of spectral power. Such simulated risers are easy to produce, are stable, and are the most common simulation result.

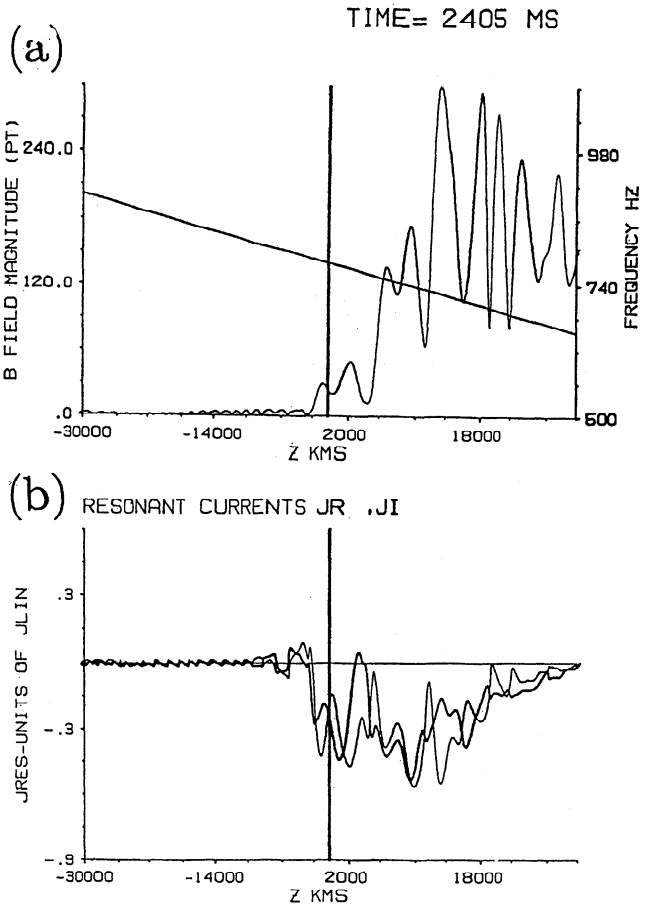

Figure 2. (a) Wave amplitude in pT, and (b) in-phase resonant particle current (J_r) and out-of-phase current (J_i in bold line) (b), as functions of z, at t=2.4 s of run A. Note the classic shape of the VLF emission generating region, and the oscillations due to sideband activity. Apart from oscillations due to sidebands, this is the classic form for trapping in a parabolic inhomogeneity (run A).

Figure 2a plots the wave field magnitude R (in pT), as a function of z at t=2.4 s. Figure 2a shows the classic shape of the quasi static GR of a triggered VLF emission [*Nunn*, 1984]. This is a nonlinear self-consistent structure which is surprisingly dynamically stable. It sits near the phase equator, and the VLF wave field propagates out to the receiver at the right boundary. The structure will undergo slow variations with time and is not absolutely static because the frequency and linear growth rates vary. Sideband activity is also chaotic and nonstationary by nature. The GR configuration that

is most dynamically stable can change with time, for example, from a riser to a faller, thus giving hooks. It is surprising that such a complex nonlinear structure should be so stable and reproducible. Something very similar, however, is observed by Geotail in the case of electrostatic waves [*Matsumoto et al.*, 1994b; *Omura et al.*, 1996].

Figure 2b shows the corresponding plot of nonlinear current as a function of z, where J_r is the component of $\tilde{J}$ in phase with $E_\perp$, and J_i is the component in phase with $B_\perp$. These curves show the characteristic form for trapping in a parabolic inhomogeneity [*Nunn*, 1974]. Apart from oscillations due to sidebands, this graph confirms that strong trapping for many trapping periods is taking place.

5.9. Simulation of a Slow Faller (Run B)

In run B we simulate the slow faller of event "F." The data for this simulation is presented in Table 2. With these parameters the resonance energy is much lower than that for run A, well within the range of the particle detector. In view of the observed low amplitude of the emission, we have assumed a linear growth rate of 50 dB/s, not far above the instability threshold. In accordance with our previous discussion F_o is assumed to have locally a functional dependence on W of the form $W^{-1.4}$. This gives a particle density in the 30~48 keV band of 0.0025/cm^3 in agreement with observations and in the 10~30 keV band a density of 0.0058/cm^3, on the low side. To fit observations $B_{\max}$ is set at 25 pT. The observed amplitude profile for event F was remarkably constant, and so in this simulation we will employ a time domain nonlinear loss process in which localized damping is applied as a function of local wave amplitude. Fallers are often observed to be highly monochromatic, and so this simulation will employ a narrow matched filter bandwidth of 12 Hz.

Figure 3 shows the f/t spectrogram of the exit wave field. The frequency resolution of the Hamming weighted FFT is 2.5 Hz. The emission is triggered by broadband

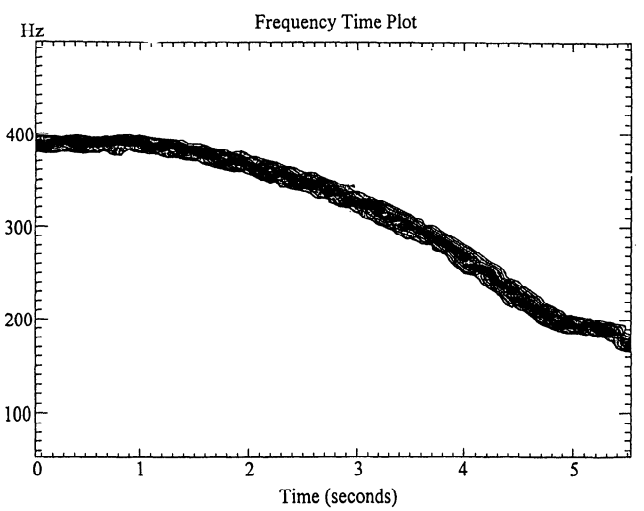

Figure 3. The f/t spectrogram of simulated slow faller (run B).

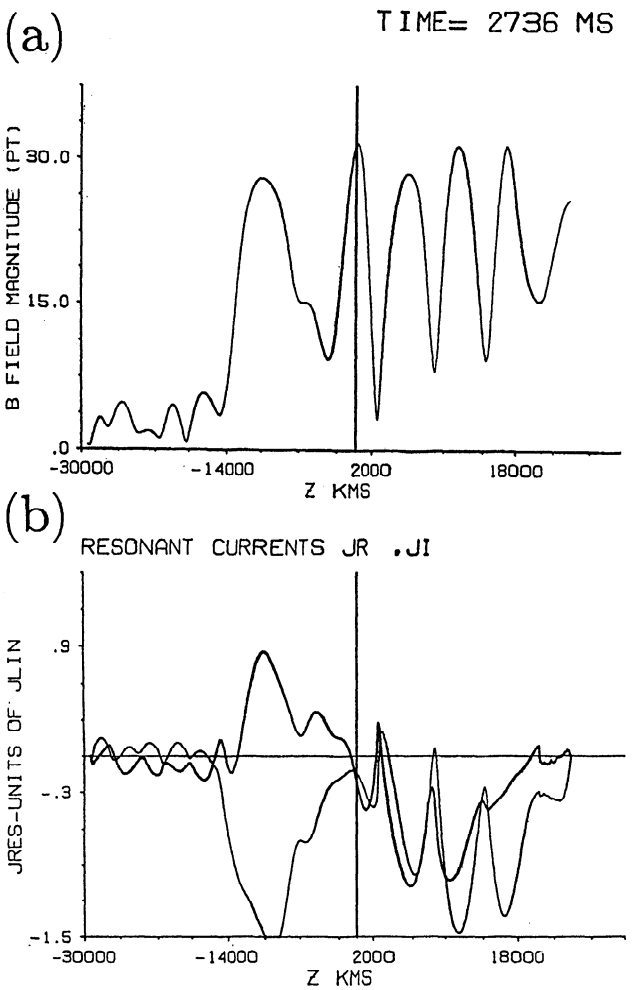

Figure 4. (a) Wave amplitude in pT, and (b) nonlinear currents J_r and J_i (in bold line) as functions of z, at t=2.7 s of run B. Note the characteristic form of currents indicative of trapping in a parabolic inhomogeneity. The emission GR is further upstream than for the riser, allowing trapping in the region $z < 0$.

noise, $B_{\rm rms} = 0.7$ pT, in the simulation band. The simulated emission falls by 200 Hz in about 5 s, in very good agreement with event F.

Figure 4a is a plot of wave field amplitude as a function of z at $t = 4.356$ s. The GR is seen to be further upstream than in the case of the riser simulation, which is contrary to the predictions by *Helliwell* [1967]. If we inspect the curves for J_r, J_i in Figure 4b we see again that they have the form indicative of strong trapping in a parabolic inhomogeneity, even though $B_{\max} = 25$ pT only. In this case there is strong trapping upstream of the "phase equator" or zero inhomogeneity point, as evidenced by positive values for J_i. This results in negative values for $\Phi = \partial/\partial z(J_i/R)$, setting up the negative frequency gradient across the simulation zone, which causes the negative sweep rate. Later in the simulation the wave envelope slips downstream, but the frequency gradient has already been set up and the frequency continues to fall according to (8). This is confirmed by Figure 5 which plots the average spatial gradient of wave

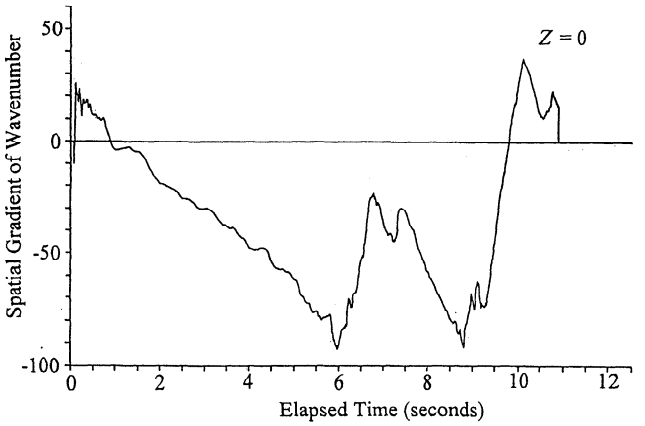

Figure 5. Plot against time of the spatial gradient of wavenumber $\partial k/\partial z V_g^2$ averaged across the simulation box. This spatial gradient is set up in the first 4 s by negative values of $\partial/\partial z(J_i/R)$, and is responsible for the falling frequency.

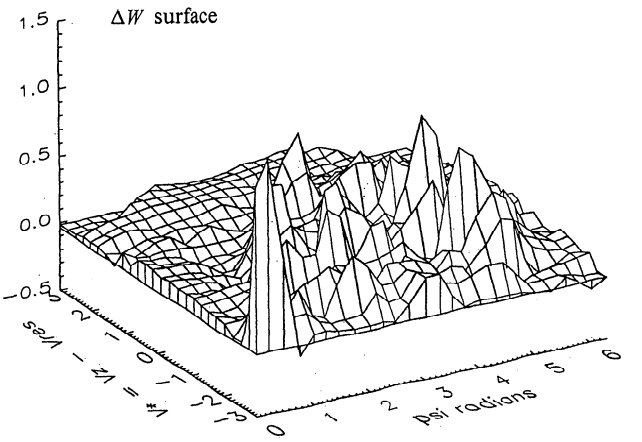

Figure 7. Wire diagram of ΔW in the $\psi - v^*$ plane at t=3 s, $\alpha = 55°$. The bunch of trapped particles with large positive ΔW is very apparent (run B)

number $\partial k/\partial z\ V_g^2$ across the simulation zone, as a function of time.

Figure 6 plots wave amplitude exiting from the phase box at $z = z_r$ and is seen to be held in the region of 20 pT, as expected. Note that since the linear growth rate is only just above the instability threshold, the nonlinear saturation mechanism is only lightly invoked.

Figure 7 is a wire diagram of ΔW in the ψ, v^* plane at $t = 3$ s, $\alpha = 55°$. Since the simulation bandwidth is very narrow, trapping dynamics are very close to simple CW theory. The bunch of stably trapped nonlinear particles are identified by large positive ΔW and are clearly visible. Geotail data appears to fit the nonlinear theory very well.

Overall, this run B gives very close agreement with the observed faller in event F. Remarkably, when the Geotail values for f, L, Ω_e, B_{max}, and N_e were input into the code, a faller with the correct sweep rate was produced at once. Very little tweeking of parameters was needed. There is little doubt that the Geotail data seems to fit the nonlinear theory very well!

5.10. Simulation of Hooks: Run C

Many simulations have been performed with the code, but space only allows one more example to be shown. Geotail observations show that hook shaped waveforms, both up and down, are not uncommon. In run C we take a large linear growth rate of 120 dB/s and trigger the code with broadband noise. A downward hook followed by an upward hook is produced. Data used for run C is given in Table 2. The purpose of this run is to show that the code can produce both types of hook and to elucidate the mechanism whereby sweep rate can change sign.

Figure 8 shows a f/t spectrogram of the exit signal. FFT resolution is 2 Hz. The relatively broad bandwidth (47 Hz) of the matched filter allows the formation of multiple sidebands, about three at any one time, with

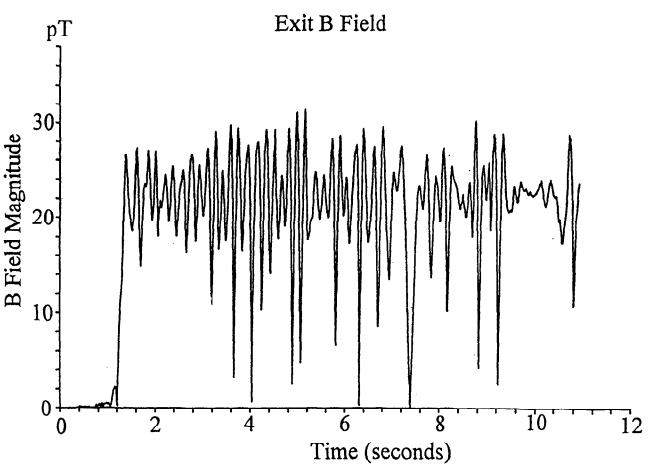

Figure 6. Exit field amplitude as a function of time (run B).

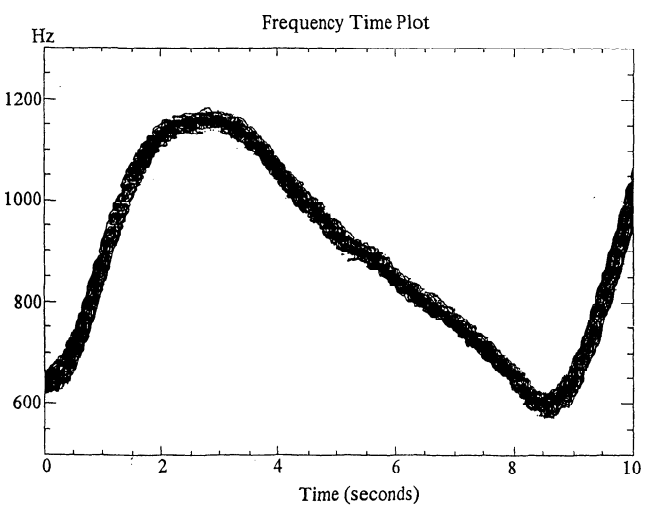

Figure 8. The f/t spectrogram of double hook shaped emission, presented as a shaded contour plot. Note the strong sideband structure (run C).

a separation of about 20 Hz. This double hook simulation reveals that there are two main types of generation region structure. One type is normally associated with a faller, and Figure 4 is a good example . The wave profile extends well upstream of the phase equator, and causes significant trapping to take place there. This results in a positive J_i and a negative value for Φ, which sets up the negative spatial gradient of k which gives rise to the falling tone. The other type of GR is seen in Figure 2, where wave amplitude is largely downstream of the phase equator, J_i is negative, and Φ is positive. This type of GR is associated with risers. In this run a riser is first produced with a GR of the riser type. As frequency rises the linear growth rate increases, causing the wave envelope to extend upstream. The GR then becomes of faller type, and negative k gradient is set up, resulting in a faller. As frequency falls, linear growth rate falls, and the GR profile slips downstream. We then have a positive Φ, and a positive k gradient is set up. From (8) this gradient is a dominant term in the expression for $\partial f/\partial t$, and hence a riser results.

6. Conclusions

The Geotail satellite skims the dayside magnetopause and on such passes usually observes VLF chorus and discrete VLF emissions. The satellite is near the generation regions of such emissions. Geotail's onboard instrumentation provides comprehensive measurements of ambient magnetic field, plasma density, five components of the EM wave field, as well as electron distribution functions up to 48 keV accumulated over a 24-s time span.

The main thrust of the paper has been to use an established 1-D EM Vlasov code to numerically simulate VLF "events" observed on Geotail. The first significant point to emerge is that the observed values of wave amplitude, ambient B field, and plasma density point towards very strong nonlinear trapping of cyclotron resonant electrons in the equatorial zone. This is even true for apparently "weak" events. Over the last 25 years a theoretical structure has been developed which explains VLF emissions in terms of nonlinear trapping of cyclotron resonant electrons. The results in this paper underline and reinforce this approach.

Simulations were run using observed parameters and the code was able to reproduce many of the observed events. Agreement with observations has been very good. For example, when the code was run with parameters observed in conjunction with an observed faller, the code produced a matching faller at once. On Geotail, risers are the most common feature observed. This is mirrored by the code which shows a strong preference towards triggering risers, when fed with average Geotail parameters. Simulated risers also matched observations quite well.

The code was found to be relatively insensitive as far as choice of unperturbed distribution function is concerned. Experiments showed that the most important parameter was linear growth rate. A value of $\gamma_{LIN} \geq 40$ dB/s was always necessary for triggering to take place, since this level of growth is required to sustain a self-consistent generation region in a constant position on a geomagnetic field line. Another requirement was that a positive gradient F_o', which is the driver for the instability process, is concentrated at pitch angles in the range $40° \sim 70°$, where particle motion is nonlinear. If these two requirements were met, the code invariably triggered. The generation region produced appeared as a very stable, nonlinear structure. The setup process was very repeatable. The code was triggered by very weak random noise, and successive runs gave a similar emission.

The condition $\gamma_{LIN} \geq 40$ dB/s is thus seen as the requirement for absolute nonlinear instability. If this is satisfied, the plasma is unstable against the formation of nonlinear VLF emissions and will immediately self-trigger to produce a discrete emission. This condition of nonlinear absolute instability contrasts with behavior in the low-amplitude linear regime where the plasma is only convectively unstable. This gives us some insight into how chorus comes about. If bouncing energetic particles produce an oscillating linear growth rate, the plasma periodically becomes absolutely unstable and immediately produces a VLF emission from ambient noise, thus giving a sequence of matching elements. Each chorus element arises spontaneously from a nonlinear instability and is either retriggered from reflected wave energy from the last element or is due to oscillating particle bunches.

Another aspect of the physics to emerge from these simulations was the mechanism responsible for rising or falling frequency. An important feature for both risers and fallers is the establishment of a gradient of wave number/frequency across the generation region. This is set up by the quantity $\Phi = \partial/\partial z(J_i/R)$, which also contributes directly to the frequency sweep rate. Generation regions were observed to be of two types. Type A is largely confined downstream of the phase equator, with $\Phi > 0$, thus giving a riser. Type B has significant amplitude upstream of the phase equator and traps electrons there. Trapping upstream of the phase equator gives $\Phi < 0$, causing a faller. Formation of hooks comes about when the GR configuration changes between these two.

One area of difficulty in matching the simulations to the Geotail data concerns the energetic electron distribution function. Observed anisotropies and particle densities give linear growth rates of ~ 10 dB/s for the 24-s averaged distribution functions. This is not enough to trigger. One can only assume that triggering is due to transient increases in flux or to gradient changes in localized regions of velocity space, which are due to either injection of particles or bouncing of particle bunches. Unfortunately, distribution functions cannot be measured on timescales of the order of 1 s. In this paper we have kept to observed particle densities, and decreased gradients with respect to energy W. It is by no means certain that this is correct, but fortunately the code is not unduly sensitive to distribution function.

It is not really surprising that 24-s average distribution functions are not above the absolute instability limit as the plasma cannot remain long in this state. Regarding future progress, the main challenge is development of 3-D codes for VLF simulations, such that artificial saturation need not be employed. This is a huge computational task which will probably need the computer technology of the next decade.

Acknowledgments. One author, D. Nunn, gratefully acknowledges being appointed to the post of Visiting Professor at RASC, where this work was undertaken. The computations were done on the KDK computer system at RASC, Kyoto University.

The Editor thanks R. A. Helliwell and K. Maeda for their assistance in evaluating this paper.

References

Burtis, W. J., and R. A. Helliwell, Magnetospheric chorus: Occurrence patterns and normalized frequency, *Planet. Space Sci., 24*, 1007, 1976.

Carlson, C. R., R. A. Helliwell, and D. L. Carpenter, Variable frequency VLF signals in the magnetosphere: Associated phenomena and plasma diagnostics, *J. Geophys. Res., 90*, 1507, 1985.

Carlson, C. R., R. A. Helliwell, and U. S. Inan, Space time evolution of whistler mode wave growth in the magnetosphere, *J. Geophys. Res., 95*, 15,073, 1990.

Chang, H. C., and U. S. Inan, Quasi-relativistic electron precipitation due to interactions with coherent VLF waves in the magnetosphere, *J. Geophys. Res., 88*, 318, 1983.

Cheng, C. Z., and G. Knorr, The integration of the Vlasov equation in configuration space, *J. Geophys. Res., 95*, 15073, 1976.

Cornilleau-Wehrlin, N., R. Gendrin, F. Lefeuvre, M. Parrot, R. Grard, D. Jones, A. Bahnsen, E. Ungstrup, and W. Gibbons, VLF electromagnetic waves observed onboard GEOS-1, *Space Sci. Rev., 22*, 371-382, 1978.

Denavit, J., Numerical simulation of plasmas with periodic smoothing in phase space, *J. Comput. Phys., 9*, 75, 1972.

Dunckel, N. and R. A. Helliwell, Whistler mode emissions in the OGO satellite, *J. Geophys. Res., 74*, 6371-6385, 1969.

Frank, L. A., K. L. Ackerson, W. R. Paterson, J. A. Lee, M. R. English, and G. L. Pickett, The comprehensive plasma instrumentation (CPI) for the GEOTAIL spacecraft, *J. Geomagn. Geoelectr., 46*, 23-37, 1994.

Frank, L. A., W. R. Paterson, and K. I. Ackerson, Plasma velocity distribution in the near-Earth plasma sheet; A first look with the Geotail spacecraft, *J. Geophys. Res., 101*, 10,627-10,637, 1996.

Helliwell, R. A., *Whistlers and Related Ionospheric Phenomena*, Stanford Univ. Press, Stanford, Calif., 1965.

Helliwell, R. A., A theory of discrete emissions from the magnetosphere, *J. Geophys. Res., 72*, 4773, 1967.

Helliwell, R. A., Controlled stimulation of VLF emissions from Siple station, Antarctica, *Radio Sci., 18*, 801, 1983.

Inan, U. S., T. F. Bell, D. L. Carpenter, and R. R. Anderson, Explorer 45 and IMP 6 observations in the magnetosphere of injected waves from the Siple station VLF transmitter, *J. Geophys. Res., 82*, 1177, 1977.

Kokubun, S., T. Yamamoto, M. H. Acuna, K. Hayashi, K. Shiokawa, and H. Kawano, The GEOTAIL magnetic field experiment, *J. Geomagn. Geoelectr., 46*, 7-21, 1994.

Matsumoto, H., I. Nagano, R. R. Anderson, H. Kojima, K. Hashimoto, M. Tsutsui, T. Okada, I. Kimura, Y. Omura, and M. Okada, Plasma wave observations with GEOTAIL Spacecraft, *J. Geomag. Geoelectr., 46*, 59-95, 1994a.

Matsumoto, H., H. Kojima, T. Miyatake, Y. Omura, M. Okada, and M. Tsutsui, Electrostatic solitary waves (ESW) in the magnetotail: BEN wave forms observed by GEOTAIL, *Geophys. Res. Lett., 21*, 2915-2918, 1994b.

Morrison, K., M. J. Engebretson, J. R. Beck, J. E. Johnson, R. L. Arnoldy, J. R. Cahill Jr., and D. L. Carpenter, A study of quasi periodic ELF VLF emissions at three Antarctic stations: Evidence for off equatorial generation, *Ann. Geophys., 12*, 139, 1994.

Mukai, T., S. Machida, Y. Saito, M. Hirahara, T. Terasawa, N. Kaya, T. Obara, M. Ejiri, and A. Nishida, The low energy particle (LEP) experiment onboard the Geotail satellite, *J. Geomagn. Geoelectr., 46*, 669-692, 1994.

Nagano, I., S. Yagitani, H. Kojima, and H. Matsumoto, Analysis of wave normal and Poynting vectors of the chorus emissions observed on Geotail, *J. Geomagn. Geoelectr., 48*, 299-307, 1996.

Nunn, D., Wave particle interactions in electrostatic waves in an inhomogeneous medium, 2, *J. Plasma Phys., 6*, 291-307, 1971.

Nunn, D., A self consistent theory of triggered VLF emissions, *Planet. Space Sci., 22*, 349-378, 1974.

Nunn, D., A quasi static theory of triggered VLF emissions, *Planet. Space Sci., 32*, 325-350, 1984.

Nunn, D., A nonlinear theory of sideband instability in ducted whistler mode waves, *Planet. Space Sci., 34*, 429, 1986.

Nunn, D., The numerical simulation of VLF nonlinear wave-particle interactions in collision-free plasmas using the Vlasov Hybrid simulation technique, *Comput. Physics Commun., 60*, 1-25, 1990.

Nunn, D., A novel technique for the numerical simulation of hot collision-free plasma: Vlasov Hybrid Simulation, *J. Comput. Phys., 108*-(1), 180-196, 1993.

Nunn, D., and A. J. Smith, The numerical simulation of whistler triggered VLF emissions observed in Antarctica, *J. Geophys. Res., 101*, 5261-5277, 1996.

Omura, Y., and H. Matsumoto, Computer simulations of basic processes of coherent whistler wave particle interactions in the magnetosphere, *J. Geophys. Res., 87*, 4435, 1982.

Omura, Y., and H. Matsumoto, Simulation study of frequency variations of VLF triggered emission in a homogeneous field, *J. Geomag. Geoelectr., 37*, 829, 1985.

Omura, Y., D. Nunn, H. Matsumoto, and M. J. Rycroft, A review of observational, theoretical and numerical studies of VLF triggered emissions, *J Atmos. Terr. Phys., 53*, 351-368, 1991.

Omura, Y., H. Matsumoto, T. Miyake, and H. Kojima, Electron beam instabilities as generation mechanism of electrostatic solitary waves in the magnetotail,. *J Geophys. Res., 101*(A2), 2685-2697, 1996.

Paschal, E. W., and R. A. Helliwell, Phase measurements of whistler mode signals from the Siple VLF transmitter, *J. Geophy. Res., 89*, 1667, 1984

Rastani, K., U. S. Inan, and R. A. Helliwell, DE-1 observations of Siple trnasmitter signals and associated sidebands, *J. Geophys. Res., 90*, 4128, 1985.

Sazhin, S. S., and M. Hayakawa, Magnetospheric chorus emissions–a review, *Planet. Space Sci., 40*, 681-697, 1992.

Tsurutani, B. T., and E. J. Smith, Two types of magnetospheric ELF chorus and their substorm dependence, *J. Geophys. Res., 82*, 5112, 1977.

Tsutsui, M., I. Nagano, H. Kojima, K. Hashimoto, H. Matsumoto, and S. Yagitani, Measurements and analysis of antenna impedance aboard the the Geotail spacecraft, *Radio Sci., 32*(3), 1101, 1996.

Williams, D. J., R. W. McEntire, C. Schlemm II, A. T. Y. Lui, G. Gloeckler, S. P. Christon, and F. Gliem, GEOTAIL energetic particles and ion composition instrument, *J. Geomagn. Geoelectr., 46*, 39-57, 1994.

Yagitani, S., I. Nagano, H. Matsumoto, Y. Omura, W. R. Paterson, L. A. Frank, and R. Anderson, Generation and propagation of chorus emissions observed by GEOTAIL in the dayside outer magnetosphere, paper presented at 1996 International Symposium on Antennas and Propagation, IEICE, Chiba, Japan, 1996.

D. Nunn, Department of Electronics and Computer Science, University of Southampton, Southampton, Hants, SO17 1BJ, UK. (e-mail: dn@ecs.soton.ac.uk)

H. Matsumoto and Y. Omura, Radio Atmospheric Science Center, Kyoto University, Uji, Kyoto, 611, Japan. (e-mail: matsumot@kurasc.kyoto-u.ac.jp; omura@kurasc.kyoto-u.ac.jp)

I. Nagano and S. Yagitani, Department of Electrical and Computer Engineering, Kanazawa University, Kanazawa, 920, Japan (e-mail: nagano@ec.t.kanazawa-u.ac.jp; yagitani@ec.t.kanazawa-u.ac.jp)

(Received May 31, 1996; revised May 23, 1997; accepted July 11, 1997.)